Simple lattice models of ion conduction: Counter ion model versus random energy model

J. Reinisch and A. Heuer
Westfälische Wilhelms-Universität Münster, Institut für Physikalische Chemie and SFB 458, Schlossplatz 4/7, 48149 Münster, Germany
(Received 21 December 2001; published 2 August 2002)

The role of the Coulomb interaction between mobile particles in ionic conductors is still under debate. To clarify this aspect we perform Monte Carlo simulations on two simple lattice models (counter ion model and random energy model) which contain the Coulomb interaction between positively charged mobile particles, moving on a static disordered energy landscape. We find that the nature of static disorder plays an important role if one wishes to explore the impact of the Coulomb interaction on the microscopic dynamics. This Coulomb-type interaction impedes the dynamics in the random energy model, but enhances dynamics in the counter ion model in the relevant parameter range.

DOI: 10.1103/PhysRevB.66.064301 PACS number(s): 66.30.Dn

I. INTRODUCTION

Many disordered insulating materials show universal behavior in their ionic dc and ac conductivity. Two prominent examples are the Arrhenius temperature dependence of the dc conductivity and the fact that ac conductivity data for different temperatures can be scaled onto a single master curve. This curve is similar for most materials. This observed universality[1,2] has stimulated research to find a common mechanism for ion conductivity in these materials. A different type of system is disordered Anderson insulators, displaying electron transport. They are denoted Coulomb glasses. In contrast to ion conductors nonlocalized dynamical processes play an important role in these systems. The nonlocalized dynamics gives rise to a very different temperature dependence of the dc conductivity at low temperatures, which turns out to be proportional to $\exp[-(T_M/T)^{1/4}]$ (Mott's law[3]) or to $\exp[-(T_0/T)^{1/2}]$ (Efros-Shklovskii law[4]).

Similar computational approaches have been chosen to investigate both types of problems and various theoretical models have been developed in this context.[5–10] The focus of this work lies on the effect of the Coulomb interaction on the microscopic dynamics in ion conductors. We chose two similar lattice models to investigate the relevant microscopic dynamics: the counter ion model[11,12] (CIM) and the random energy model with cation-cation interaction (REM),[13] which has some features in common with the Coulomb glass model used for the second group of disordered solids.[9,10] The CIM and REM are designed to reflect important aspects of vitreous ion conductors, which are a high degree of disorder and mobile charged ions in a fixed glass network. The models differ in the way the time-independent (static) disorder is realized. In this paper we analyze the effects of the Coulomb interaction among mobile ions and show that the nature of the disorder has great influence on the dynamics. In Sec. II we present the models as well as computational details, while in the Sec. III the results are presented and discussed.

II. MODELS AND COMPUTATIONAL DETAILS

A. Similarities of both models

Both models are based on a single type of mobile particles restricted to discrete sites in a simple cubic lattice with l^3 sites of distance a. The distance for a single jump is limited to a, and occupied positions are forbidden. All mobile particles have the same positive charge. In contrast to other works on the CIM,[11,12] the strength of the Coulomb interaction between the mobile particles can be varied independently from the strength of static disorder by an appropriate selection of parameters, as is also possible for the REM; see below for precise definitions. This variation is essential to elucidate the effect of the Coulomb interaction among the mobile particles on their dynamics. There are two energy contributions to the total Hamiltonian: mobile particles moving on a time-dependent potential surface (generated by the particles themselves) and on a time-independent potential surface. We call the first dynamic and the latter static. The dynamic part has the same form in both models and the Hamiltonian for the cation-cation interaction is

$$H_{cat}=\frac{1}{2}\sum_{i\neq i'}\frac{n_i n_{i'} e^2}{r_{ii'}}. \tag{1}$$

A configuration with sites i is described by the occupation numbers $n_i=1$ for occupied sites and $n_i=0$ for empty sites. The omitted factor $4\pi\epsilon_0$ is taken into account by use of appropriate units. The mean nearest-neighbor interaction in a system with randomly distributed cations can be written as

$$V_c=\frac{e^2}{r_s}. \tag{2}$$

Here r_s is the mean distance of nearest neighbors in such a system with cation concentration $c=N/l^3$,

$$r_s=3\sqrt{\frac{3}{4\pi c}}. \tag{3}$$

Furthermore we introduce the dimensionless parameter Γ_{cat} via

$$\Gamma_{cat}=\frac{V_c}{k_B T}=\frac{e^2}{k_B T r_s}. \tag{4}$$

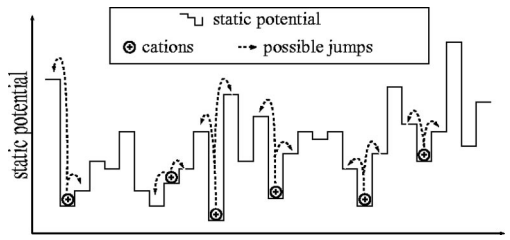

FIG. 1. One-dimensional illustration of the static potential landscape in the random energy model. The arrows indicate possible jumps.

In the literature this parameter is already established for the REM (Ref. 13) and we use it for the CIM to ensure comparability. The Hamiltonian for the cation interaction can thus be rewritten as

$$\frac{H_{cat}}{k_B T} = \Gamma_{cat} \frac{H_{cat}}{V_c}. \tag{5}$$

In what follows V_c is regarded as a constant for a given concentration. Here $\Gamma_{cat} \propto e^2$ is a measure for the interaction strength between the cations relative to $k_B T$.

B. Static disorder in the random energy model

The REM features a straightforward approach of the principle of representing complexity by randomness. Each site i gets a random energy taken from a Gaussian distribution with standard deviation σ_ϵ and mean value 0. The Hamiltonian for the static disorder becomes

$$H_{stat} = \sum_i n_i E_i^{static}. \tag{6}$$

The model is fully determined by two dimensionless parameters: σ_r is connected to the standard deviation of the random site energies by

$$\sigma_r = \frac{\sigma_\epsilon}{k_B T}. \tag{7}$$

In changing σ_r one can change the strength of static disorder relative to temperature in the system. As before, the second parameter Γ_{cat} determines the cation-cation interaction strength. The total Hamiltonian reads

$$\frac{H}{k_B T} = \Gamma_{cat} \frac{H_{cat}}{V_c} + \frac{H_{stat}}{k_B T}. \tag{8}$$

In Fig. 1 the potential landscape of the REM is illustrated.

C. Static disorder in the counter ion model

In the CIM static disorder is generated by randomly placing negatively charged particles at centers of cubic lattice cells. As for cations these anions cannot occupy the same site. The resulting potential landscape (see Fig. 2) is different from that seen in Fig. 1. As for the REM we used Γ_{cat} to control the interaction strength among cations and defined a

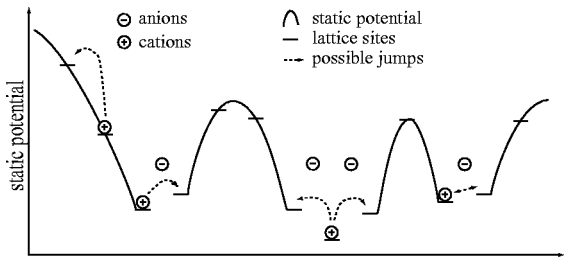

FIG. 2. One-dimensional illustration of the static potential landscape in the counter ion model. The arrows indicate the possible jumps.

parameter Γ_{stat} adequate to control the interaction strength between cations and anions. It is defined in analogy to Γ_{cat} as

$$\Gamma_{stat} = \frac{k_{ca} V_c}{k_B T}. \tag{9}$$

The factor k_{ca} has been introduced to vary the strength of the cation-anion interaction separately from the cation-cation interaction. For $k_{ca} = 1$ and thus $\Gamma_{cat} = \Gamma_{stat}$ one recovers the standard choice of parameters for the CIM. In contrast to previous works we wish to break with charge neutrality and rather interpret H_{stat} as a general static-disordered energy landscape. Thus Γ_{stat} can be varied in analogy to σ_r, thereby modifying the strength of the disorder. The total Hamiltonian for the CIM is

$$\frac{H}{k_B T} = \Gamma_{cat} \frac{H_{cat}}{V_c} + \Gamma_{stat} \frac{H_{stat}}{V_c}. \tag{10}$$

D. Computational settings

The number of lattice sites in one dimension was set to 20 for all data throughout this work. For simulating bulk properties we apply periodic boundary conditions and the minimum image convention.[14] As shown in Fig. 3 the smallness of the finite-size effects justifies our choice of 20 lattice sites per dimension. All presented data were calculated with a cation concentration of 0.03. The number of anions for generating the static energy landscape in the CIM was kept identical to the number of cations. The contributions of the Cou-

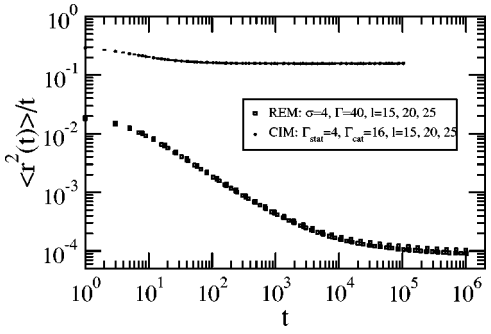

FIG. 3. Typical errors and finite-size effects for both models. The largest errors are of the size of the symbols and occur at large t.

lomb interaction were calculated via Ewald summation. The number of different starting configurations ranges from 5 to 10. This rather small number made it possible to simulate a large range of parameters. For model systems with $c=0.03$ and $e^2=1$, which were used throughout this paper, one has $V_c=0.501$.

III. RESULTS

The diffusion constants are taken from $\langle r^2(t)\rangle/t$ data. Figure. 3 shows some examples. Each curve begins with a short-time plateau changes into a dispersive regime from t_1 to t_2 and forms a long-time plateau beyond t_2. In the dispersive regime between t_1 and t_2 the curve follows a Jonscher-type[15] power law

$$\langle r^2(t)\rangle/(6t)\sim t^{k'-1}. \tag{11}$$

The following relations are used to determine the diffusion constants:

$$6D(t)=\langle r^2(t)\rangle/t,$$

$$6D_{dc}=\lim_{t\to\infty},\langle r^2(t)\rangle/t,$$

$$6D_{ac}=\lim_{t\to 0}\langle r^2(t)\rangle/t.$$

The high-frequency diffusion constant D_{ac} was also calculated from the average hopping rate $a^2\langle w\rangle=6D_{ac}$. For details on the general behavior of the REM and the CIM, see Refs. 13,12, and 16.

In the REM the presence of a cation-cation interaction leads to a significant decrease in diffusion and an increase in dispersion.[13] A quantitative analysis of the behavior can be found in Ref. 17. For a REM without a long-range Coulomb interaction, i.e., $\Gamma_{cat}=0$, the activation energy E_a can be calculated as the difference between the Fermi energy and the critical percolation energy.[7,17] For a concentration of 0.03 the Fermi energy is $-1.88\sigma_\epsilon$ and the percolation energy is $-0.49\sigma_\epsilon$. Hence the activation energy is $-0.49\sigma_\epsilon+1.88\sigma_\epsilon=1.39\sigma_\epsilon$. This reasoning is only valid for low temperatures $\sigma_r\gg 1$. For high temperatures $\sigma_r\ll 1$ it can be shown[17] that the activation energy is roughly equal to $\sigma_\epsilon/\sqrt{\pi}=0.56\sigma_\epsilon$. Here we analyze the REM including the long-range Coulomb interaction for which this analytical treatment is no longer possible. Simulated data for various Γ_{cat} and σ_r are shown in Fig. 4 (left). The data for $\Gamma_{cat}=0$ correspond to a vanishing cation-cation interaction and the regression for the low-temperature regime leads to an activation energy of $1.41\sigma_\epsilon$ which is in good agreement with the theoretical value resulting from percolation arguments; see above. One can easily see that the low-temperature part of all curves can be approximated fairly well by straight lines. The first data point for $\sigma_r=0$ is omitted for all Γ_{cat}. Interestingly, the change of slope at high temperatures, i.e., small σ_r, as predicted for $\Gamma_{cat}=0$, seems to hold for the large cation-cation interaction, too. The data shown in Fig. 4 (left) can be fitted with the activation energy dependent on σ_r, Γ_{cat}, and a cross term $\Gamma_{cat}\sigma_r$,

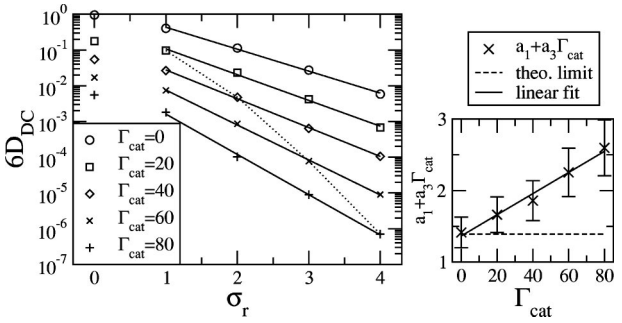

FIG. 4. Left: dependence of the low-frequency diffusion constant D_{dc} on σ_r in the REM. The lines correspond to exponential fits; the data for $\sigma_r=0$ are omitted. The dotted line describes the temperature dependence of D_{dc} for a constant quotient $\sigma_r/\Gamma_{cat}=\sigma_\epsilon/V_c=0.05$. The errors are smaller than the symbol size. Right: dependence of the slope on Γ_{cat}. The data match the theoretical limit at $\Gamma_{cat}=0$.

$$\ln[6D_{dc}]=-(a_1\sigma_r+a_2\Gamma_{cat}+a_3\sigma_r\Gamma_{cat}). \tag{12}$$

The slope of the fits in Fig. 4 (left) can be expressed according to Eq. (12) as $a_1+a_3\Gamma_{cat}$. Figure 4 (right) illustrates this dependence. The three coefficients turn out to be $a_1=1.41$, $a_2=0.063$, and $a_3=0.015$. The nonvanishing value of a_3 is of particular interest since it contradicts the conclusions of Maass *et al.*[17] They showed that for $c=0.01$ the low-temperature behavior is activated, i.e., $\ln[6D]\propto 1/T$ when varying the temperature. Since $\sigma_r\propto 1/T$ and $\Gamma_{cat}\propto 1/T$, this statement is identical to $a_3=0$. We have included a curve in Fig. 4 (left) which represents a variation of the temperature only; this curve shows a proportionality to $A/T+B/T^2(A,B>0)$. In contrast to this result experimental data for low temperatures show no curvature[17] or opposite curvature.[18] This temperature dependence is also very different to that observed in Coulomb glass for which, if at all, a description with $B<0$ would be appropriate for a limited temperature regime in order to recover the Efros-Shklovskii law.

Furthermore we also analyzed the dependence of D_{ac} on Γ_{stat} and Γ_{cat}. Figure 5 shows data for D_{ac} in analogy to those in Fig. 4 (left). Exponential fits are not as accurate as for D_{dc}. Though the data cannot be accurately fitted as straight lines an approximated slope is decreasing with increasing Γ_{cat}. Thus D_{ac} has a different behavior as compared to D_{dc}.

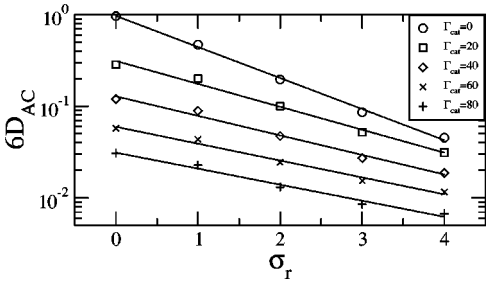

FIG. 5. Dependence of the high-frequency diffusion constant D_{ac} on σ_r in the REM. The lines are exponential fits and serve as guides to the eye. The errors are within the symbol size.

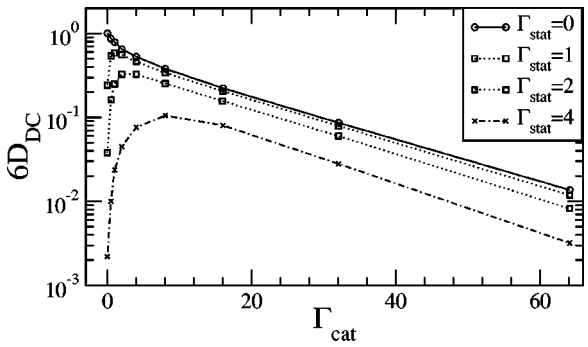

FIG. 6. Dependence (CIM) of the low-frequency diffusion constant D_{dc} on Γ_{cat}. The maximum ($\Gamma_{cat,max}$) shifts to larger Γ_{cat} for higher values of Γ_{stat}. The errors are smaller than the symbols.

The analysis for the CIM was performed in a similar way. The first surprising feature is the increase in mobility of the cations for D_{dc} (Fig. 6) and D_{ac} (Fig. 7) when increasing Γ_{cat} from 0 with fixed Γ_{stat}. This is the completely opposite behavior as compared to the REM. Increasing Γ_{cat} further leads to an increase in diffusion until a maximum is reached; from this maximum the diffusion decreases and the slope becomes constant in a logarithmic plot. Obviously, a simple functional form such as Eq. (12) cannot be found for the CIM. A difference between D_{dc} and D_{ac} is that $\Gamma_{cat,max}$ for D_{dc} is approximately equal to Γ_{stat} whereas $\Gamma_{cat,max}$ for D_{ac} increases more rapidly with Γ_{stat}.

The different behavior of the REM as compared to the CIM can be rationalized by a closer inspection of the differences in the potential surfaces. Comparing Fig. 1 and Fig. 2 and taking the definitions of the models into account, it is evident that the static potential of a lattice site in the CIM surface is spatially correlated, whereas in the REM no correlation among adjacent sites exists. This correlation in the CIM has a direct consequence: Figure 8 illustrates a correlation of the static potential of a lattice site with the mean value of the dynamic potential. For a single starting configuration the static energy of each site is constant during simulation, being denoted as E_{static}/k_BT in Fig. 8. The mean value of the dynamic energy $\overline{E}_{dynamic}$ at some site is generated by averaging over all energies which a particle at this site has due to H_{cat} during a simulation. The observed correlation in Fig. 8 (left) indicates a correlation of H_{cat} and H_{an}; high cation-cation energy corresponds to low static energy and vice versa. It could be shown that the three regions observed in the CIM correspond to three different types of lattice sites. There are sites with no, one, or two adjacent anions, i.e., anions with a distance of $\sqrt{3}(a/2)$. No such correlation is observed for the REM.

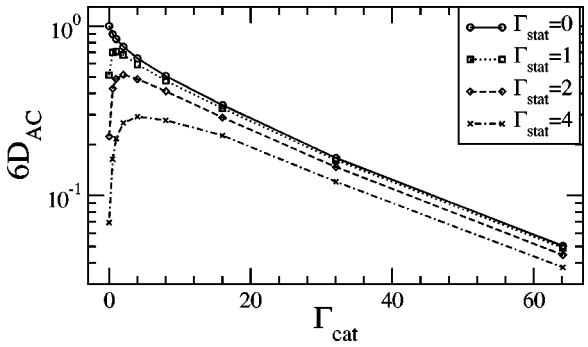

FIG. 7. Dependence (CIM) of the high-frequency diffusion constant D_{ac} on Γ_{cat}. The maximum ($\Gamma_{cat,max}$) shifts to larger Γ_{cat} for higher values of Γ_{stat}. The errors are smaller than the symbols.

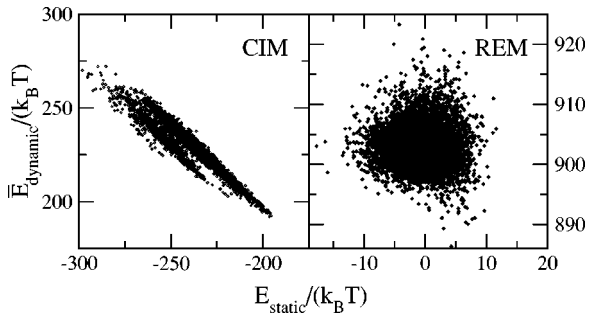

FIG. 8. Correlation between static potential and mean value of the dynamic potential for the CIM (left: $\Gamma_{cat}=10$, $\Gamma_{stat}=10$) and the REM (right: $\Gamma_{cat}=40$,$\sigma_r=4$). Each site is represented by a single diamond symbol (20^3 for each graph). In the CIM a strong correlation is observed; the slope is close to 1. In the REM no significant correlation is observed.

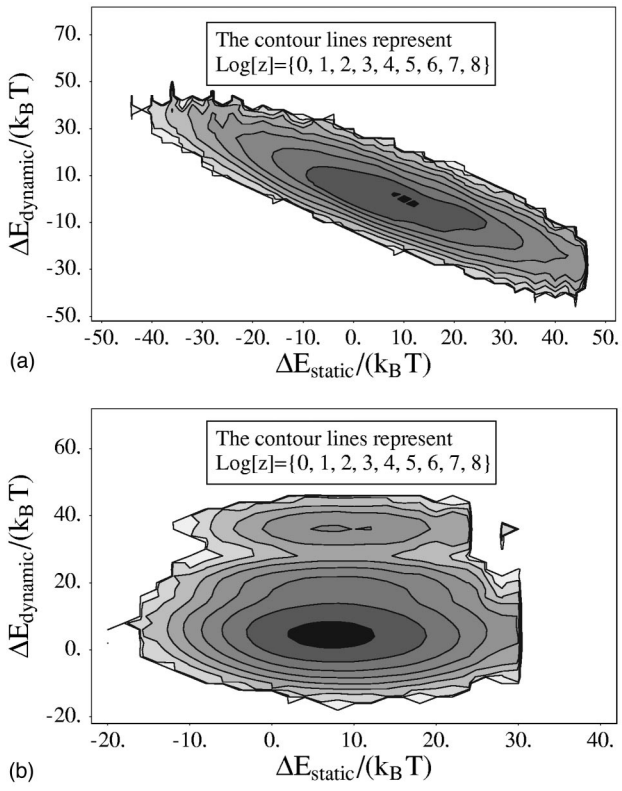

FIG. 9. Matrices of successful and unsuccessful trial jumps in the CIM (top, $\Gamma_{cat}=\Gamma_{stat}=10$) and the REM (bottom, $\sigma_r=4$, $\Gamma_{cat}=40$) resolved for static and dynamic jump energies. z is a counter of how many jumps happen per energy interval during a simulation run. The choice of parameters has no influence on the qualitative picture.

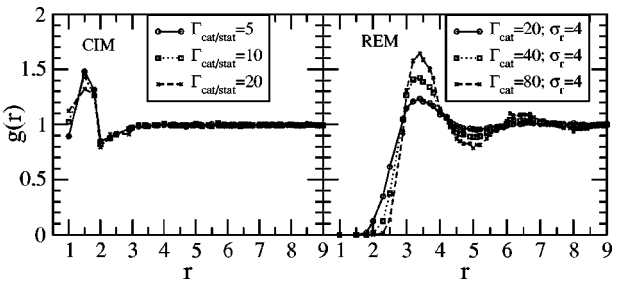

FIG. 10. Radial density function $g(r)$ for the CIM(left) and the REM(right). For the CIM the parameters are chosen to show the temperature dependence and for the REM the dependence of $g(r)$ on Γ_{cat}. The errors are within the size of the symbols.

To elucidate the impact of this correlation on the ion dynamics, all occurring trial jumps, accepted or not by the Metropolis algorithm, were recorded during a Monte Carlo simulation with respect to their static (ΔE_{static}) and dynamic ($\Delta E_{dynamic}$) jump energy differences (Fig. 9). The sum of ΔE_{static} and $\Delta E_{dynamic}$ is the total energy difference for a jump. One apparent effect of the correlation for the CIM is quite obvious: a high-energy contribution from the static energy is accompanied by a low-energy contribution from the dynamic energy and vice versa. Therefore to first approximation the total energy does not change during a jump, giving rise to faster dynamics. The REM does not show this behavior. For the REM both contributions are independent and both impede the cation dynamics. A consequence is a different jump energy distribution in the CIM as compared to the REM. To further explore the reasons for this behavior the radial density function $g(r)$ of both models is illustrated in Fig. 10. Obviously, the cations in the REM have a structure; they prefer a certain distance to each other which returns periodically in the graph. This structure is very similar to that found in simple liquid systems. The CIM does not show such a structure; instead it shows an unusual high concentration of cations in very short distances and beyond $r \approx 3$ the bulk density is already reached. The found structures give possible explanations for the observed behaviors: In the REM each cation is surrounded by a cage of other cations, and this cage slows down the movement[19] because most moves would increase H_{cat}. In the CIM the cations prefer to populate low-energy positions around the anions, which results in an effective screening of the anion charge. This screening flattens the overall energy landscape and thus gives rise to increased mobility. Increasing Γ_{cat} reduces the clustering due to cation-cation repulsion but also supports screening due to higher cation charge. These two effects compete and may account for the observed behavior; see Fig. 6 and Fig. 7.

We are now able to reason the parameter dependence of Eq. (12) for the REM. The first term arises from the static disorder of the energy landscape. The second term is introduced by a cage effect as mentioned above. The cross term on the other hand has no single microscopic origin for D_{dc} and D_{ac}. For D_{dc} it may arise from relaxation of the system to a small perturbation (i.e., a cation jump). By a jump process a cation may have left a well-adjusted environment and is surrounded by an energetically unfavorable environment. Apart from jumping back the total system may also adjust to this new situation as already formulated in the concept of mismatch and relaxation by Funke *et al.*[5,2] The situation at the new position improves energetically after some time due to the subsequent relaxation of the adjacent particles, thereby reducing the probability of a backjump with time. In the presence of disorder this neighbor relaxation is, of course, much slower since also the neighbors experience the effect of static disorder. Therefore it is more likely for the central particle to jump back, giving rise to a decrease of D_{dc} due to the simultaneous effect of static disorder and the cation-cation interaction. For D_{ac} an increase in Γ_{cat} reduces the dependence on σ_r and therefore the above argumentation fails. For no cation interaction and in the limit of zero temperature the cations occupy only the N lowest sites in static energy. By introducing a cation interaction the emerging liquid structure forces the particles to occupy also some sites which are higher in static energy (but lower in total energy); this would lead to the observed reduction in σ_r dependence.

IV. SUMMARY

The REM and CIM display major qualitative differences in their dependences of D_{ac} and D_{dc} on the system parameters. We gave qualitative reasoning by taking a closer view of the microscopic origins as the effects of caging, relaxation, screening, and disorder were observed. We have also shown that the conduction in the REM does not show simple Arrhenius behavior and despite their similarities the REM behaves quite differently as compared to the Coulomb glass due to the different nature of the trial moves. The results of this work give rise to a new important variable in disordered solids: the spatial correlation of the potential energy hypersurface. Currently we are analyzing the energy hypersurface of real ion conductors to extract this important piece of information.

ACKNOWLEDGMENTS

We wish to acknowledge the support of the DFG (SFB 458) as well as helpful discussions with R. Banhatti, P. Maass, and B. Roling. We acknowledge additional support by B. Roling for providing us the Ewald summation program.

[1] J.C. Dyre and T.B. Schrøder, Rev. Mod. Phys. **72**, 873 (2000).
[2] K. Funke, C. Cramer, and B. Roling, Glass Sci. Technol. (Amsterdam) **73**, 244 (2000).
[3] N.F. Mott, J. Non-Cryst. Solids **1**, 1 (1968).
[4] A.L. Efros and B.I. Shklovskii, J. Phys. C **8**, L49 (1975).
[5] K. Funke, Solid State Ionics **94**, 27 (1997).
[6] J. Summerfield and B.N. Butcher, Philos. Mag. B **49**, L65 (1984).
[7] J.C. Dyre, Phys. Rev. B **48**, 12 511 (1993).

[8] J.C. Dyre, Phys. Rev. B **47**, 9128 (1993).
[9] M. Pollak and M. Ortuño, *Elektron-Elektron Interactions in Disordered Systems* (North-Holland, Amsterdam, 1985).
[10] B.I. Shklovskii and A.L. Efros, *Elektronic Properties of Doped Semiconductors* (Springer, Berlin, 1984).
[11] W. Dieterich, D. Knödler, and P. Penzig, J. Non-Cryst. Solids **172–174**, 1237 (1994).
[12] D. Knödler, P. Penzig, and W. Dieterich, Solid State Ionics **86–88**, 29 (1996).
[13] P. Maass, J. Peterson, A. Bunde, W. Dieterich, and H.E. Roman, Phys. Rev. Lett. **66**, 52 (1991).
[14] N. Metropolis, A.W. Rosenbluth, A.H. Teller, and E. Teller, J. Chem. Phys. **21**, 1087 (1953).
[15] A.K. Jonscher, *Dielectric Relaxation in Solids* (Chelsea Dielectric Press, London, 1983).
[16] P. Penzig and W. Dieterich, Solid State Ionics **105**, 209 (1998).
[17] P. Maass, M. Meyer, A. Bunde, and W. Dieterich, Phys. Rev. Lett. **77**, 1528 (1996).
[18] H. Namikawa, J. Non-Cryst. Solids **14**, 88 (1974).
[19] B. Doliwa and A. Heuer, Phys. Rev. Lett. **80**, 4915 (1998).